BIOCHEMISTRY
including biophysical chemistry & molecular biology

Article

pubs.acs.org/biochemistry

Quantum Mechanics/Molecular Mechanics Studies of the Mechanism of Falcipain-2 Inhibition by the Epoxysuccinate E64

Kemel Arafet, Silvia Ferrer,* Sergio Martí, and Vicent Moliner*

Departament de Química Física i Analítica, Universitat Jaume I, 12071 Castelló, Spain

Supporting Information

ABSTRACT: Because of the increasing resistance of malaria parasites to antimalarial drugs, the lack of highly effective vaccines, and an inadequate control of mosquito vectors, the problem is growing, especially in the developing world. New approaches to drug development are consequently required. One of the proteases involved in the degradation of human hemoglobin is named falcipain-2 (FP2), which has emerged as a promising target for the development of novel antimalarial drugs. However, very little is known about the inhibition of FP2. In this paper, the inhibition of FP2 by the epoxysuccinate E64 has been studied by molecular dynamics (MD) simulations using hybrid AM1d/MM and M06-2X/MM potentials to obtain a complete picture of the possible free energy reaction paths. A thorough analysis of the reaction mechanism has been conducted to understand the inhibition of FP2 by E64. According to our results, the irreversible attack of Cys42 on E64 can take place on both carbon atoms of the epoxy ring because both processes present similar barriers. While the attack on the C2 atom presents a slightly smaller barrier (12.3 vs 13.6 kcal mol^{-1}), the inhibitor−protein complex derived from the attack on C3 appears to be much more stabilized. In contrast to previous hypotheses, our results suggest that residues such as Gln171, Asp170, Gln36, Trp43, Asn81, and even His174 would be anchoring the inhibitor in a proper orientation for the reaction to take place. These results may be useful for the rational design of new compounds with higher inhibitory activity.

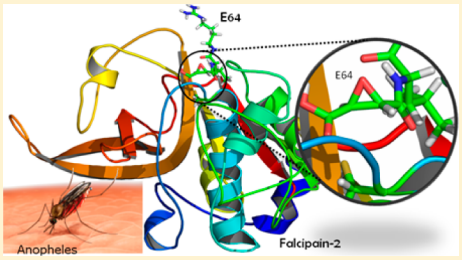

Malaria is an infectious disease that, in humans, is caused by five species of parasites of the genus *Plasmodium*: *Plasmodium falciparum*, *Plasmodium vivax*, *Plasmodium ovale*, *Plasmodium malariae*, and *Plasmodium knowlesi*. Malaria caused by *P. falciparum* is the most deadly form and that caused by *P. vivax* the most extended; the other three species are found much less frequently. Malaria parasites are transmitted to humans by the bite of infected female mosquitoes of more than 30 anopheline species. Globally, an estimated 3.4 billion people were at risk of malaria in 2012, with children under five years of age and pregnant women most severely affected.[1] Almost half of the world's population permanently lives under risk of infection where malaria is endemic. Because of the increasing resistance of malaria parasites to antimalarial drugs, the lack of highly effective vaccines, and an inadequate control of mosquito vectors, the problem is growing, especially in the developing world. New approaches to drug development are consequently required.[2,3]

In *P. falciparum*, various proteases catalyze the degradation of human hemoglobin, and the amino acids derived from this process are incorporated into parasite proteins or utilized for energy metabolism.[4] One of the proteases involved in this metabolic process is named falcipain-2 (FP2). FP2, belonging to the family of cysteine proteases (papain-like enzymes known as clan CA), is expressed during the erythrocytic stage of the life cycle of the parasite,[5] and the inhibition of these has proven to be indispensable for the complete blockage of parasitic growth and proliferation.[6] FP2 has emerged as a promising target for the development of novel antimalarial drugs.[6−8]

In the past several years, various types of FP2 inhibitors have been reported to be capable of inactivating the enzyme;[9−15] however, only a few structures reported in the Protein Data Bank correspond to the crystal structure of FP2 with its inhibitors.[16−18] One of them is the crystal structure of FP2 complexed with *N*-[*N*-(1-hydroxycarboxyethylcarbonyl)-leucylaminobutyl]guanidine, E64 (see Scheme 1), the first epoxysuccinyl discovered and a natural potent and specific irreversible inhibitor of cysteine proteases. One advantage of this type of inhibitors is their stability under physiological conditions toward simple thiols. In addition, although they have limited selectivity toward different cysteine proteases, their reactivity toward cysteine proteases and not other proteases, along with their chemical unreactivity, makes this class of inhibitors useful as pharmaceutical agents.[19] E64 was isolated from a culture of *Asperigillus japonicas*,[20] and its structure was determinated by Hanada et al. in 1978.[21] E64 contains a *trans* (2*S*,3*S*)-configured epoxide ring, whereas the amino acid residues of the peptidyl part of the inhibitor have the L-configuration. The substituents at C2 and C3 on the epoxide ring are in *trans* position to one another,[22,23] which appears to be crucial because the *cis* configuration leads to a total loss of inhibition activity. E64 inhibits cysteine proteases by S-alkylation of the active site cysteine, which results in the

Received: January 14, 2014
Revised: April 25, 2014
Published: May 8, 2014

dx.doi.org/10.1021/bi500060h | *Biochemistry* 2014, 53, 3336−3346

Scheme 1. General Mechanism of the Inhibition of Cysteine Proteases by the Epoxysuccinate E64[a]

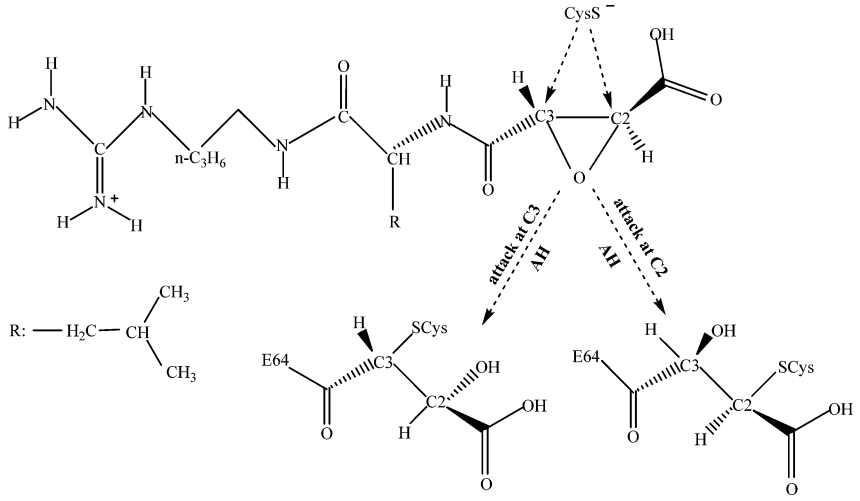

[a]AH is a source of protons.

opening of the epoxide ring (see Scheme 1) and stabilization of the protein−inhibitor complex.[24,25] Nevertheless, there are some open questions related to the molecular mechanism, because it appears that the attack can take place at either C2 or C3 depending on the orientation of the epoxysuccinate in the active site.[26] On one hand, it has been demonstrated by X-ray investigations that the attack of the alkylation step with epoxide takes place at C2 when an acid is the C2 substituent on this carbon.[17,27−31] The regiospecificity and inhibition potency of epoxide- and aziridine-based inhibitors were studied by theoretical methods by Engels and co-workers who, on the basis of the exploration of potential energy surfaces (PES) obtained with hybrid quantum mechanics/molecular mechanics (QM/MM) potentials, proposed the attack at C2 as being more favorable.[32] On the other hand, Bihosky, in an experimental study of the rate and regioselectivity of reactions between 2,3-epoxy carbonyl compounds and methanethiolate in solution, observed that the rate constant for both attacks differs by a factor of only 2, with the C3 attack preferred ($k_{C2\text{-attack}}$ = 0.0036 min^{-1}, and $k_{C3\text{-attack}}$ = 0.0064 min^{-1}).[33]

An insight into the molecular mechanism of cysteine proteases inhibition by epoxy inhibitors shows that an important feature is the fact that the stereochemistry of the enzyme−inhibitor adduct suffered an inversion of configuration at the reaction site because of a nucleophilic attack by the active site thiolate in an S_N2 reaction.[26] For instance, E64, which has the 2*S*,3*S* configuration before the nucleophilic attack, assumes the 2*R*,3*R* configuration after the covalent bond between the cysteine residue and C2 is formed.[26]

Another matter of debate is the nature of the catalytic acid on the active site. It was initially postulated that when E64 inhibits papain, the oxirane ring would be protonated by His159.[34] Varughese and co-workers[35] rejected this suggestion, on the basis of the crystal structure of papain inhibited by E64. They suggest that the epoxide was more likely to be protonated by a water molecule because of the large distance between the resulting hydroxyl group and His159. Meara and co-workers in mechanistic studies based on the experimental determination of rate constants and the pH dependence of inhibition confirmed that His159 is not necessary for protonation of the epoxide and that water is the predominant source of protons; these results are likely to be general for all epoxysuccinyl inhibitors with a free carboxylate bound to the C2 atom.[36]

The principal aim of this paper is to gain insights into the inhibition of FP2 by the epoxysuccinate E64 based on molecular dynamics (MD) simulations using hybrid QM/MM methods,[37] which have been shown to be a valuable tool for studying biomolecular systems.[38−40] These calculations allow us to obtain a complete picture of the possible free energy reaction paths, including details of the reaction mechanism, their corresponding free energy barriers and averaged geometries, and interactions between the inhibitor and the protein. Analysis of the results can contribute to our understanding of the inhibition of FP2 by E64, information that can be used to rationally design new inhibitors.

COMPUTATIONAL MODEL

The initial coordinates for building our molecular model were taken from the X-ray crystal structure of FP2 inhibited by E64 from *P. falciparum* with PDB entry 3BPF[17] at 2.90 Å resolution. The selected structure contains one polymer of four chains, each chain consisting of 241 amino acids (FP2), the inhibitor E64, 10 water molecules, and one glycerol molecule (see Figure 1). Some missing residues of the structure (Pro189, Leu190, Thr191, Lys192, and Lys193) were added by homology with the crystal structure of FP2 from *P. falciparum* with PDB entry

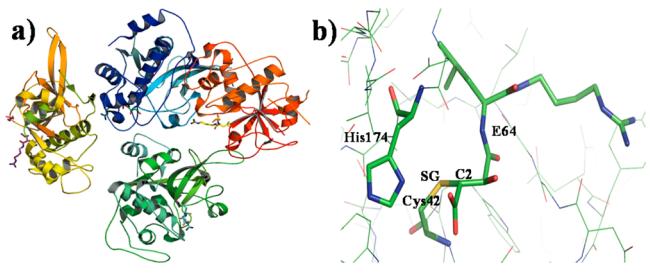

Figure 1. (a) Full tetramer 3BPF structure showing four chains that compose the crystal structure of FP2 inhibited by E64 from *P. falciparum*. (b) Detail of the active site where the inhibitor (C2 atom of E64) binds to the enzyme (SG atom of residue Cys42). E64 and Cys42 are represented as thick sticks.

dx.doi.org/10.1021/bi500060h | *Biochemistry* 2014, 53, 3336−3346

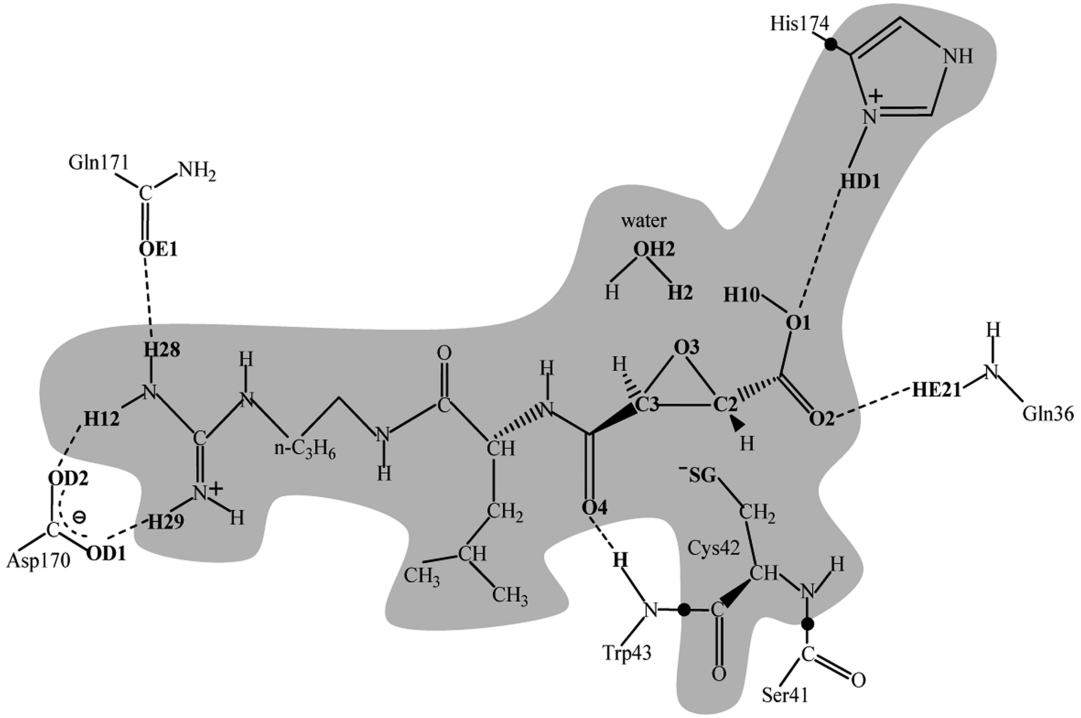

Figure 2. Details of the active site corresponding to the studied model. The gray region corresponds to the QM region, including the inhibitor E64, the side chain of Cys42, a water molecule, and the imidazole ring of His174. The link atoms between the QM and the MM regions are denoted with black dots. The labels of the atoms correspond to the X-ray crystal structure of FP2 inhibited by E64 from *P. falciparum*.

2GHU.[41] In our model, we took only a monomer (chain A) from the tetramer.

Hydrogen atoms were added to the crystal structure of FP2 inhibited by E64 from *P. falciparum* (a productlike structure) using the fDYNAMO library.[42] In this way, the question of the protonation state of Cys42 is initially avoided. The pK_a values of the structure of PDB entry 3BPF were calculated via the empirical PROPKA 3.1 program of Jensen et al.[43−45] at a physiological pH. According to the results, Glu67, Glu69, and His174 had to be protonated while His19, His27, and His197 were set up as being neutral. A total of six counterions (Na^+) were placed into optimal electrostatic positions around the system, to obtain electroneutrality. Keeping in mind that the digestive vacuole where FP2 is found has a pH of 5.5, we also studied the protonation of the system at this pH to check the influence of pH on the protonation state of the protein. According to PROPKA calculations, a change from pH 7 to 5.5 would affect only four residues: His19, His27, Asp91, and His197. These residues are located 30.7, 28.2, 15.7, and 29.8 Å, respectively, from the C2 atom of the epoxy ring of the inhibitor. These large distances suggest that no significant differences would be expected in the short pH range from 5.5 and 7. Nevertheless, we have performed QM/MM MD simulations on reactant and product states at both protonation states (see Table S1 of the Supporting Information), confirming this assumption and, consequently, indicating that our calculations can be considered as representative of the reaction taking place in the digestive vacuole. Finally, the full system was placed in an orthorhombic box of water molecules (80 Å × 80 Å × 100 Å).

The QM region was described by means of the AM1d semiempirical Hamiltonian,[46] while the rest of the protein and water molecules were described by OPLS-AA[47] and TIP3P[48] force fields, respectively, implemented in the fDYNAMO library.[42] To saturate the valence of the QM/MM frontier, we used the link atom procedure.[49,50] The number of QM atoms then became 78 and includes the full inhibitor E64, the side chain of Cys42, a water molecule, and the imidazole ring of His174 (see Figure 2). The final system contains a total of 61048 atoms. Because of the size of the system, all residues more than 25 Å from the C1 atom of the inhibitor were kept frozen (54048 atoms of a total of 61048). To treat the nonbonding interactions, a switch function with a cutoff distance in the range of 14.5−18 Å was used. All the QM/MM calculations were conducted using the fDYNAMO library.[42]

The system was relaxed for 700 ps by means of QM/MM MD at 300 K using the *NVT* ensemble and the Langevin−Verlet integrator. Interestingly, two different conformations, differing in the relative orientation of the E64 in the active site of the protein, were detected: a conformation similar to the initial X-ray structure (PDB entry 3BPF) with the guanidine group of E64 interacting with Tyr78 and a conformation in which the guanidine group of E64 interacts with Asp170 (see Figure 3). Analysis of the time evolution of the potential energy and the total energy obtained during the last 200 ps of the QM/MM MD simulation performed for productlike structures in the two different conformations (see Figure S1 of the Supporting Information) reveals that both structures were stable. Root-mean-square fluctuations of backbone atoms of the protein and atoms of E64 were 0.05 and 0.16 Å for the former and 0.03 and 0.15 Å for the latter, respectively. These results confirm that the system was equilibrated in both conformations. Nevertheless, according to the energetic values, the second structure (Figure 3b) appears to be more stable than the original one. Structures obtained after relaxation were used to compute hybrid AM1d/MM PESs. Stationary structures (including reactants, products, intermediates, and transition state structures) were located and characterized by means of

dx.doi.org/10.1021/bi500060h | *Biochemistry* 2014, 53, 3336−3346

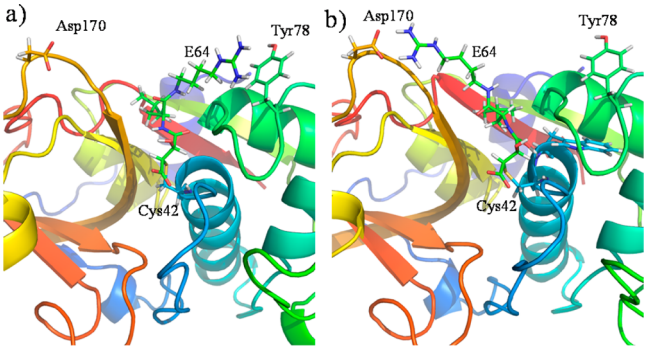

Figure 3. Representative snapshots of the two possible conformations concerning the relative orientation of E64 in the active site. (a) Conformation corresponding to the initial X-ray structure (PDB entry 3BPF) with the guanidine group of E64 interacting with Tyr78. (b) Conformation corresponding to the guanidine group of E64 interacting with Asp170.

the micromacro iterations scheme[51] starting from both productlike conformations. It is important to point out that the reactant state corresponds to the Cys42 as a thiolate anion. According to previous studies based on exploration of QM/MM potential energy surfaces of the mechanism for the addition of the Cys42 thiol to an α,β-unsaturated ester, Grazioso et al. showed that activation of Cys42 by His174 is not the rate-limiting step.[52]

Potentials of mean force (PMFs) generated as a function of a distinguished reaction coordinate (RC) were obtained using the weighted histogram analysis method (WHAM) combined with the umbrella sampling approach.[53,54] In particular, the first step of the mechanism involves the attack of sulfur on either C2 or C3 of the epoxide ring, so a one-dimensional PMF (1D-PMF) was obtained as a function of a RC, $d(CX-O3)-d(SG-CX)$ (with CX being C2 and C3), where 41 and 46 series of simulation windows for the C2 and C3 attacks were required, respectively. After that, the mechanism in which C3 is attacked leads to an intermediate, so two sources for the O3 protonation have been explored: the carboxylic group of the inhibitor and a water molecule. In the first case, the 1D-PMF was calculated using $d(O1-H10)-d(O3-H10)$ as the RC, and in the second case, the 1D-PMF was calculated using $d(OH2-H2)-d(O3-H2)$ as the RC. This required 87 and 96 series of simulations, respectively. Additionally, to investigate a possible mechanism in which the attack of the proton on O3 of the ring takes place prior to the sulfur attack, we explore three sources of the proton: His174, a water molecule, and an intramolecular transfer from the acid group at C2. The 1D-PMF was calculated using the antisymmetric combination of the $d(O3-H10)-d(O1-H10)$ distance as the RC for an intramolecular transference, the $d(O3-H2)-d(OH2-H2)$ distance as the RC for a protonation by a water molecule, and the $d(O3-HD1)-d(ND1-HD1)$ distance as the RC for a protonation by His174. These 1D-PMFs required 55, 81, and 60 simulation windows, respectively. In all the simulations, the value of the force constant used for the harmonic umbrella sampling was 2500 kJ mol^{-1} $Å^{-2}$, and the windows consisted of 20 ps of equilibration and 40 ps of production, with a time step of 1 fs. Afterward, 200 ps of AM1d/MM MD simulations on the stationary points of the free energy surfaces was performed to analyze the average properties of the key states.

Finally, to correct the low-level AM1d energy function used in the PMF, an interpolated correction scheme developed in our laboratory was applied.[55] In this correction scheme, based on a method proposed by Truhlar and co-workers for dynamical calculations of gas phase chemical reactions,[56] the new energy function employed in the simulations is defined as

$$E = E_{LL/MM} + S[\Delta E_{LL}^{HL}(\zeta)] \quad (1)$$

where S denotes a spline function, whose argument $\Delta E_{LL}^{HL}(\zeta)$ is a correction term taken as the difference between single-point calculations of the QM subsystem using a high-level (HL) method, in this case the hybrid M06-2X[57] with the 6-31+G(d,p)[58] basis set, following the suggestions of Truhlar and co-workers.[57,59] The AM1d Hamiltonian was the low-level (LL) method. The correction term is expressed as a function of the distinguished reaction coordinate ζ (RC). These calculations were conducted using Gaussian09.[60]

Scheme 2. Proposed Molecular Mechanism As Deduced from the Exploration of the PESs Corresponding to the Attack of Cys42 on C2 or C3 of the Epoxy Ring of the E64 Inhibitor

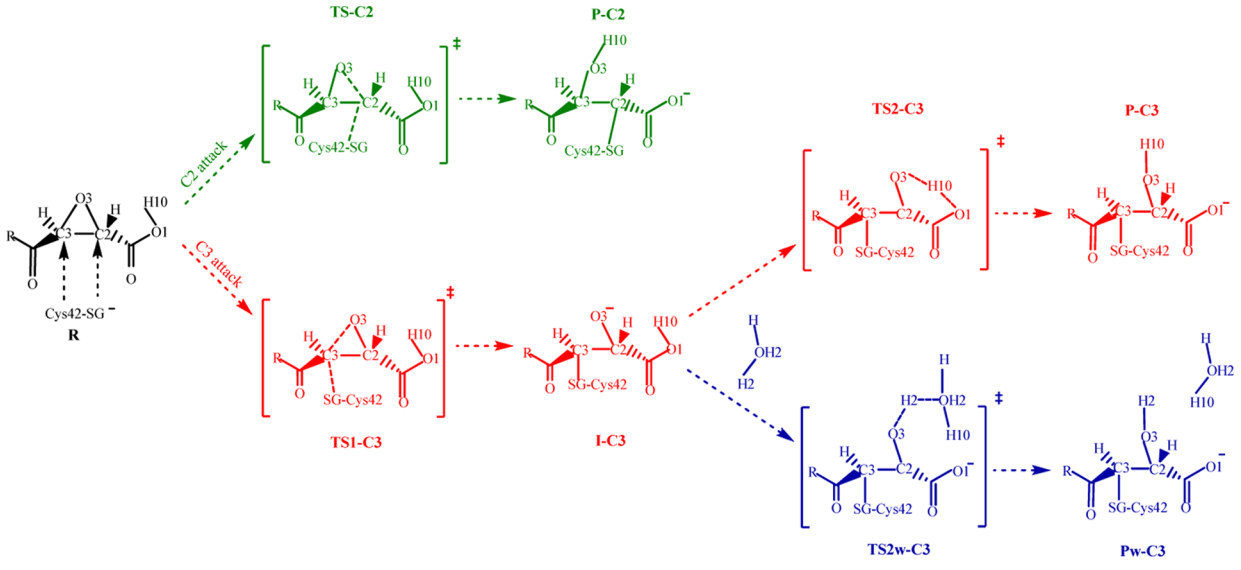

dx.doi.org/10.1021/bi500060h | Biochemistry 2014, 53, 3336−3346

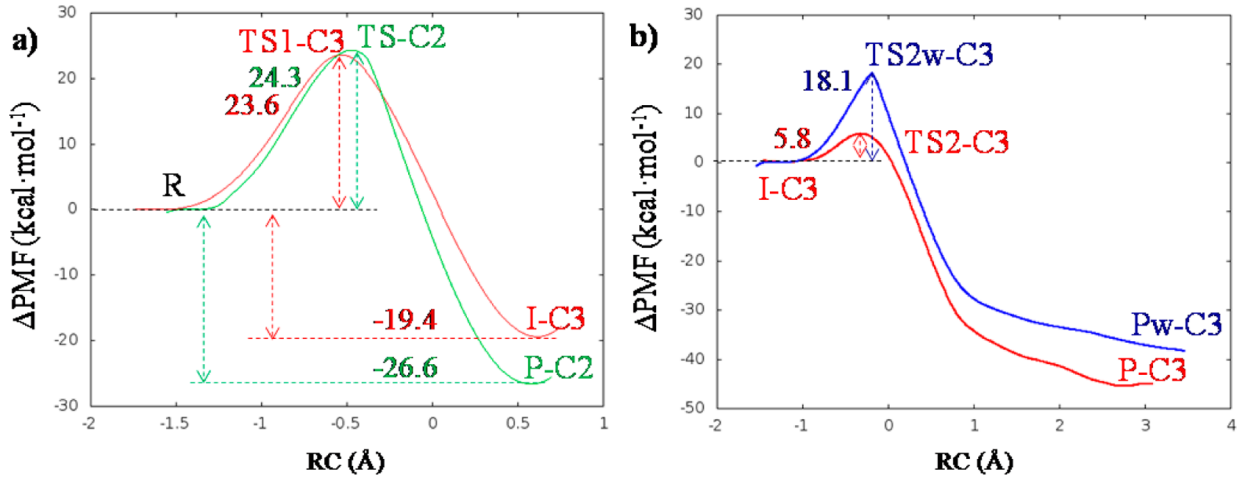

Figure 4. AM1d/MM PMFs of (a) the attack of sulfur on C2 (green line) or C3 (red line) and ring opening. RC corresponds to $d(CX-O3)-d(SG-CX)$, with *CX* being C2 or C3. (b) Transfer of a proton from the carboxylic group to O3 (intramolecular transference, red line) and from a water molecule (blue line). RC corresponds to $d(O1-H10)-d(O3-H10)$ for the direct transfer of a proton from the carboxylic group (red line) and $d(OH2-H2)-d(O3-H2)$ for the transfer of a proton through a water molecule (blue line).

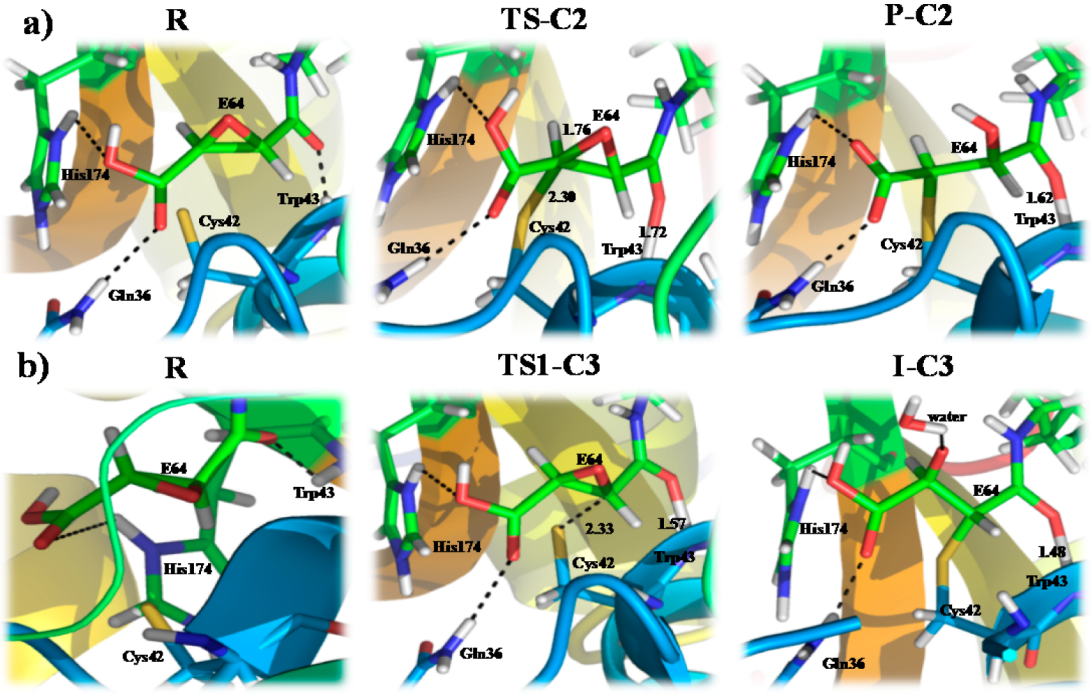

Figure 5. Representative snapshots of the key states of the reaction mechanism of inhibition of FP2 by attack of Cys42 on (a) C2 and (b) C3. Average distances are reported in angstroms.

RESULTS AND DISCUSSION

The mechanism of the inhibition of FP2 by E64 has been studied by exploring the PESs corresponding to the two possible mechanisms, the sulfur attack of conserved residue Cys42 on C2 or C3 of the epoxide ring (see Scheme 2).

According to the stationary points located on the PESs, the attack of Cys42 on C2 of the epoxy ring of the E64 inhibitor and its protonation would proceed by a single step (see the green path in Scheme 2). In this step, controlled by TS-C2, the SG−C2 bond forms in a concerted fashion with the O3−C2 bond breaking and the transfer of H10 from the carboxylic acid to O3. This was confirmed by tracing the IRC path from the located TS-C2 to reactant and product valleys. On the other hand, the mechanism of the attack on C3 proceeds in a stepwise manner through a stable intermediate I-C3 where the cysteine is covalently bonded to the inhibitor and O3 is deprotonated (see the red path in Scheme 2). From the I-C3 intermediate, H10 is transferred from the carboxylic acid to O3. Keeping in mind the fact that water molecules are present in the active site of the FP2, we explored this transfer considering two hypotheses: a direct transfer of H10 and a transfer with the participation of a water molecule (colored blue in Scheme 2).

Once the PESs had been fully explored, they were used as the starting point to generate the free energy surfaces that will allow us to gain deeper insight into the mechanisms, as well as kinetic magnitudes that can be directly compared with experimentally measured rate constants. Thus, as explained in the previous section, two 1D-PMFs were obtained for the attack of Cys42

dx.doi.org/10.1021/bi500060h | *Biochemistry* 2014, 53, 3336−3346

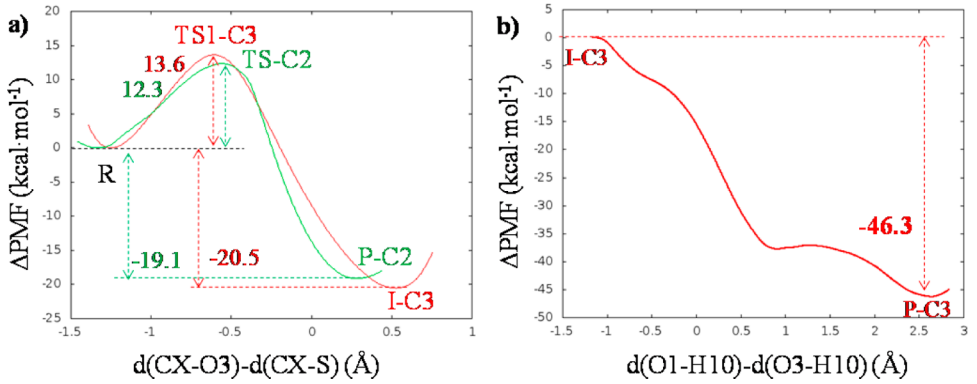

Figure 6. Free energy profiles, computed in terms of potential mean force at the M06-2X/6-31+G(d,p) level. (a) Attack of sulfur on C2 (green line) or C3 (red line) and ring opening. (b) Transfer of a proton from the carboxylic group to O3.

on C2 or C3 of the epoxide ring as a function of an antisymmetric combination of the distances defining the breaking and forming bonds, d(C*X*−O3)−d(SG−C*X*) with C*X* being C2 and C3, depending on the reaction. The PMF of the step corresponding to the transformation from I-C3 to products was calculated using the antisymmetric combination d(O1−H10)−d(O3−H10) as the reaction coordinate for the direct transfer from the carboxylic group, and using the antisymmetric combination d(OH2−H2)−d(O3−H2) as the reaction coordinate to explore the possibility of a water molecule being the source of protonation of O3. According to the AM1d/MM results, presented in Figure 4, the free energy barrier of the attack of Cys42 on C2 (24.3 kcal/mol) is very close to the free energy barrier of the first step of the mechanism of the attack on C3 (23.6 kcal/mol). The corresponding free energy profiles obtained for the conformation of E64 interacting with Tyr78 (Figure 3a) render significantly higher barriers (see Figure S2 of the Supporting Information). This, together with previous analysis of energies of both conformations, suggests that the conformation with E64 interacting with Asp170 appears to be the most stable one. Thus, all simulations and analysis were performed on the basis of this structure after its determination. Snapshots of representative average structures of the states appearing along the different reaction paths are shown in Figure 5 (snapshots of representative structures of the rest of the stationary points are shown in Figures S3 and S4 of the Supporting Information). The free energy barrier of the transformation from I-C3 to P-C3 is much lower and, considering the exothermic character of the first step, will not contribute to limiting the kinetics of the full process. As observed in Figure 4b, comparison of free energy barriers of this second step reveals that the transfer of H10 from the carboxylic group to O3 of the epoxy ring will clearly occur in a direct way without participation of a water molecule (5.8 kcal/mol vs 18.1 kcal/mol).

Thus, according to the relative energies of TS-C2 and TS1-C3, our results would be in good agreement with the experimental data of Bihosky.[33] Using the transition state theory at 300 K, his values of the rate constant ($k_{C2\text{-attack}}$ = 0.0036 min^{-1}, and $k_{C3\text{-attack}}$ = 0.0064 min^{-1}) can be translated into almost indistinguishable free energy barriers, 23.4 and 23.0 kcal/mol, respectively, which in turn are almost coincident with our predictions for TS-C2 (24.3 kcal/mol) and TS1-C3 (23.6 kcal/mol). Nevertheless, we must keep in mind the fact that the experiments of Bihosky were conducted with nonpeptidic compounds in solution with only one substituent on C2. On the other hand, because the semiempirical Hamiltonian used in our calculations can render inaccurate barriers, a correction of the profile at the DFT level of theory with the M06-2X functional was conducted (see the previous section for details). The resulting corrected profiles, presented in Figure 6, show a dramatic reduction of the barrier to 12.3 and 13.6 kcal/mol for the attack on C2 and C3, respectively, and a barrier-less process from I-C3 to products. Again, we predict similar DFT/MM free energy barriers for the rate-limiting step of both reactions, in agreement with the very similar rate constants measured by Bihosky in solution.[33] The difference in free energy barriers for attack on C2 and C3 is not as dramatic as the difference in the potential energy barriers deduced from the PESs obtained by Engels and co-workers, who obtained reaction barriers of 1 and 17 kcal/mol for the attack of cysteine on C2 and C3 of the epoxy ring of the E64c inhibitor, respectively.[32]

With regard to the second step of the mechanism of the attack of sulfur on C2, corrections were made at the M06-2X/MM level only for the direct protonation step of O3 from carboxylate group because it was clearly favored with respect to the transfer through a water molecule. In this profile (Figure 6b), a shoulder is observed in the region of products corresponding to a change in the new O3-H10 hydroxyl group. This, initially oriented to the carboxylate group of the inhibitor, points to Asn181 in the most stable product conformation. Keeping in mind that our reactions were conducted in the enzyme, we expected a significant reduction of the barrier by comparison with results obtained in solution. Importantly, our new results predict a very small preference for the attack at C2 over that at C3. Our results differ significantly from those of previous computational studies of Engels and co-workers who, based on QM/MM potential energy profiles, obtained a barrier for the C3 attack of ∼15 kcal/mol, but an almost barrier-less process for the attack on C2 of the E64c inhibitor. Nevertheless, from a thermodynamic point of view, our calculations predict a more stable enzyme−inhibitor complex when Cys42 attacks C3 than when it attacks C2, which can be deduced from the reaction free energies derived from the profiles shown in Figures 4 and 6.

An alternative mechanism of the inhibition of FP2 with E64 consisting of a protonation of the epoxy O3 atom prior to the Cys42 attack and the epoxy ring opening has been also explored. This alternative route was studied just for the attack on C2 because this is the mechanism presenting a lower barrier. Three possible sources of protons have been considered: a water molecule, protonated His174, and a direct intramolecular

dx.doi.org/10.1021/bi500060h | *Biochemistry* 2014, 53, 3336−3346

Scheme 3. Alternative Mechanisms of the Inhibition of FP2 with E64, with an Early Proton Attack on O3 of the Epoxide Ring

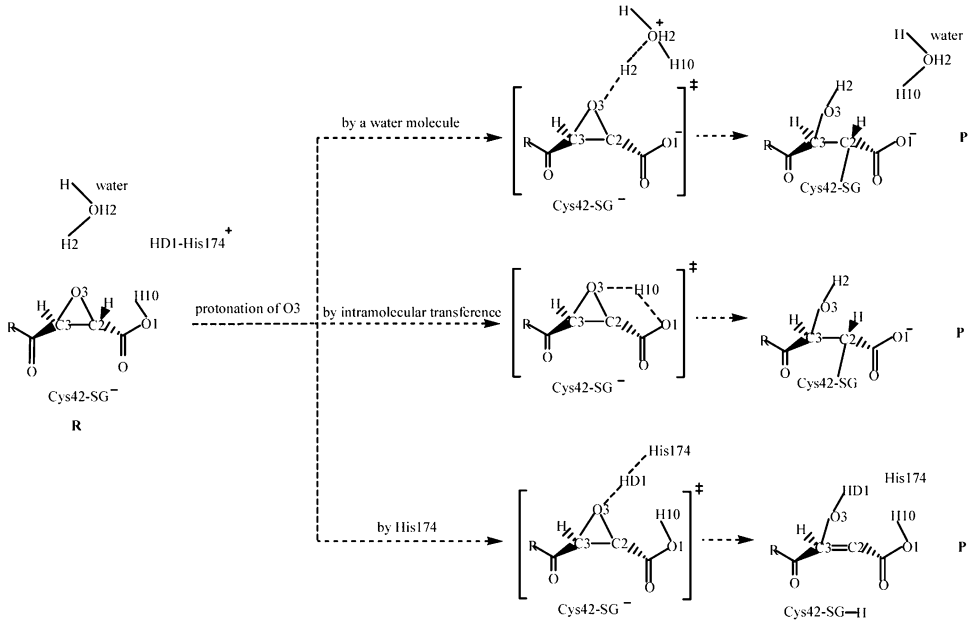

Table 1. Averaged AM1d/MM Distances Obtained for Key States Located along the Reaction Mechanism of Inhibition of FP2 by Attack of Cys42 on C2 (a) and C3 (b)[a]

(a) Attack of Sulfur on C2 of the E64 Epoxy Ring			
	R	TS-C2	P-C2
SG−C2	2.83 ± 0.03	2.30 ± 0.03	1.80 ± 0.03
O3−C2	1.44 ± 0.03	1.76 ± 0.04	2.37 ± 0.05
O3−H10	3.85 ± 0.41	2.74 ± 0.43	0.97 ± 0.03
O1−H10	0.96 ± 0.02	0.98 ± 0.03	4.09 ± 0.39
O1−HD1 (His174)	2.61 ± 0.26	2.95 ± 0.20	2.55 ± 0.23
O2−HE21 (Gln36)	3.47 ± 0.47	2.53 ± 0.24	2.25 ± 0.25
O3−H (H_2O)	2.55 ± 0.18	2.54 ± 0.13	2.70 ± 0.15
O3−H (H_2O)	2.95 ± 0.18	2.81 ± 0.13	2.81 ± 0.12
O3−H (H_2O)	3.02 ± 0.30	2.90 ± 0.23	2.63 ± 0.13
O4−H (Trp43)	3.21 ± 0.78	1.72 ± 0.27	1.62 ± 0.27
H10−O (Asn81)	6.13 ± 0.37	6.17 ± 0.36	2.36 ± 0.38
H29−OD1 (Asp170)	1.64 ± 0.10	1.64 ± 0.10	1.65 ± 0.10
H12−OD2 (Asp170)	1.62 ± 0.09	1.64 ± 0.09	1.66 ± 0.10
H28−OE1 (Gln171)	2.18 ± 0.19	2.15 ± 0.19	2.16 ± 0.19

(b) Attack of Sulfur on C3 of the E64 Epoxy Ring					
	R	TS1-C3	I-C3	TS2-C3	P-C3
SG−C3	3.01 ± 0.04	2.33 ± 0.03	1.81 ± 0.04	1.81 ± 0.04	1.80 ± 0.03
O3−C3	1.44 ± 0.03	1.89 ± 0.03	2.42 ± 0.05	2.38 ± 0.05	2.42 ± 0.05
O3−H10	3.24 ± 0.16	2.87 ± 0.27	2.47 ± 0.31	1.41 ± 0.03	0.97 ± 0.03
O1−H10	0.97 ± 0.03	0.98 ± 0.03	0.98 ± 0.03	1.12 ± 0.02	3.74 ± 0.21
O1−HD1 (His174)	3.26 ± 0.34	2.89 ± 0.18	2.96 ± 0.31	4.26 ± 0.27	2.57 ± 0.21
O2−HE21 (Gln36)	4.64 ± 0.77	2.60 ± 0.25	2.15 ± 0.18	3.22 ± 0.67	2.23 ± 0.21
O2−HD1 (His174)	5.02 ± 0.37	4.00 ± 0.20	3.81 ± 0.27	2.63 ± 0.36	4.00 ± 0.20
O3−H (H_2O)	3.91 ± 0.60	2.76 ± 0.13	2.61 ± 0.20	3.18 ± 0.70	2.92 ± 0.24
O3−H (H_2O)	3.92 ± 0.55	2.73 ± 0.10	2.93 ± 0.14	3.21 ± 0.44	2.89 ± 0.15
O3−H (H_2O)	4.13 ± 0.54	2.72 ± 0.19	2.64 ± 0.24	2.97 ± 0.20	2.38 ± 0.23
O4−H (Trp43)	4.97 ± 1.01	1.57 ± 0.24	1.48 ± 0.26	3.39 ± 1.71	1.59 ± 0.28
O4−H (Ala175)	2.78 ± 0.78	4.40 ± 0.34	4.48 ± 0.39	3.12 ± 1.05	4.56 ± 0.37
H10−O (Asn81)	3.50 ± 1.09	3.50 ± 1.09	5.00 ± 0.56	3.43 ± 0.52	2.65 ± 0.18
H29−OD1 (Asp170)	1.63 ± 0.10	1.64 ± 0.10	1.66 ± 0.10	1.65 ± 0.10	1.65 ± 0.10
H12−OD2 (Asp170)	1.62 ± 0.09	1.65 ± 0.09	1.68 ± 0.10	1.66 ± 0.10	1.67 ± 0.10
H28−OE1 (Gln171)	2.18 ± 0.19	2.15 ± 0.19	2.17 ± 0.19	2.17 ± 0.19	2.15 ± 0.19

[a]All values are in angstroms and were obtained from 200 ps of AM1d/MM MD simulations on the stationary points of the free energy surfaces.

dx.doi.org/10.1021/bi500060h | *Biochemistry* 2014, 53, 3336−3346

Table 2. Averaged AM1d/MM Mulliken Charges Obtained for Key States Located along the Reaction Mechanism of the Inhibition of FP2 by Attack of Sulfur of Cys42 on C2 (a) and C3 (b)[a]

(a) Attack of Sulfur on C2 of the E64 Epoxy Ring			
Mulliken charge	R	TS-C2	P-C2
C2	−0.094 ± 0.028	−0.053 ± 0.024	−0.481 ± 0.035
C3	−0.093 ± 0.021	0.031 ± 0.027	−0.021 ± 0.017
SG	−0.592 ± 0.163	−0.600 ± 0.061	0.267 ± 0.047
O3	−0.267 ± 0.021	−0.546 ± 0.030	−0.367 ± 0.017
H10	0.228 ± 0.018	0.228 ± 0.018	0.270 ± 0.010
O1	−0.488 ± 0.027	−0.479 ± 0.022	−0.690 ± 0.025
O2	−0.523 ± 0.077	−0.416 ± 0.027	−0.635 ± 0.030
O4	−0.429 ± 0.030	−0.510 ± 0.034	−0.539 ± 0.038

(a) Attack of Sulfur on C3 of the E64 Epoxy Ring					
Mulliken charge	R	TS1-C3	I-C3	TS2-C3	P-C3
C2	−0.132 ± 0.024	0.065 ± 0.040	0.224 ± 0.029	0.092 ± 0.031	−0.032 ± 0.019
C3	−0.125 ± 0.038	−0.016 ± 0.026	−0.542 ± 0.045	−0.506 ± 0.041	−0.512 ± 0.033
SG	−0.900 ± 0.061	−0.567 ± 0.066	0.219 ± 0.051	0.259 ± 0.050	0.271 ± 0.046
O3	−0.256 ± 0.022	−0.532 ± 0.023	−0.606 ± 0.025	−0.607 ± 0.016	−0.356 ± 0.017
H10	0.265 ± 0.015	0.293 ± 0.011	0.319 ± 0.020	0.365 ± 0.009	0.263 ± 0.010
O1	−0.436 ± 0.030	−0.491 ± 0.020	−0.484 ± 0.029	−0.523 ± 0.026	−0.697 ± 0.022
O2	−0.341 ± 0.042	−0.437 ± 0.025	−0.570 ± 0.032	−0.620 ± 0.029	−0.639 ± 0.025
O4	−0.422 ± 0.026	−0.516 ± 0.036	−0.422 ± 0.026	−0.501 ± 0.074	−0.536 ± 0.042

[a]All values were obtained from 200 ps of AM1d/MM MD simulations on the stationary points of the free energy surfaces.

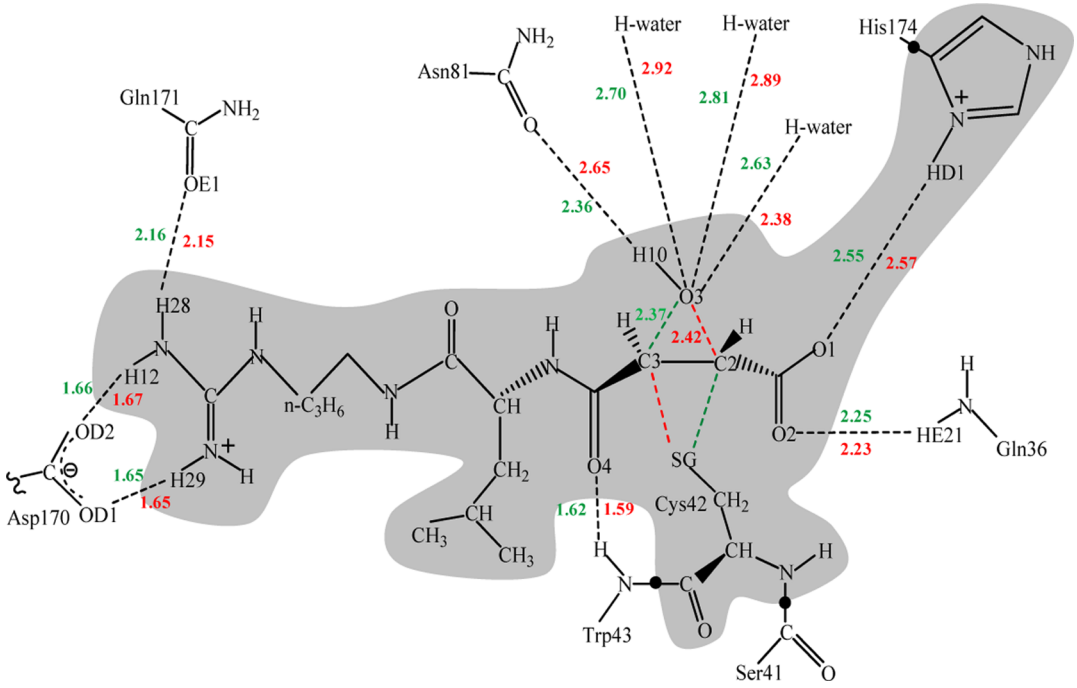

Figure 7. Schematic representation of the interactions between QM and MM parts obtained in the inhibitor−protein complex: P-C2 (green numbers) and P-C3 (red numbers). All interaction distances are in angstroms. Only distances of <3.00 Å are reported.

transfer of a proton from the carboxylic group of the inhibitor (see Scheme 3). After the required calculations had been performed to determine the free energy profiles in terms of 1D-PMFs, the corresponding free energy barriers are 65.9, 45.4, and 47.4 kcal/mol, respectively (see full PMFs in Figure S5 of the Supporting Information). Consequently, this proposed mechanism does not seem to be feasible.

Once the energetics of possible mechanisms of the inhibition of FP2 with E64 by the attack of Cys42 on C2 or C3 of the inhibitor epoxy ring had been discussed, geometrical and charge population analysis could be conducted to gain deeper insight into the origins of the formation of the FP2−E64 complex. Thus, average values of key interatomic distances of the different states located along the reaction paths on both reactions are listed in Table 1, and Mulliken charges on key atoms are listed in Table 2. A schematic representation of the inhibitor−protein complex structures obtained in the exploration of both mechanisms (P-C2 and P-C3) is depicted in Figure 7. Values of the second step of the attack of Cys42 on C3, the protonation of O3 by a water molecule, are reported as Supporting Information (Table S2).

dx.doi.org/10.1021/bi500060h | *Biochemistry* 2014, 53, 3336−3346

The first conclusion that can be drawn from values listed in Table 1 is that the distance between the sulfur atom of Cys42 and the carbon atom of the inhibitor, C2 or C3, is equivalent in the TSs with an uncertain deviation: 2.30 ± 0.03 and 2.33 ± 0.03 Å for TS-C2 and TS1-C3, respectively. Nevertheless, ring opening is in a more advanced stage of the reaction in the latter as deduced from the distance between the epoxy ring oxygen atom and the attacked carbon atom (O3−C3 and O3−C2 distances of 1.89 and 1.76 Å, respectively). This is related to the distance between the O3 atom and the hydrogen atom initially located on the carboxylate group of the inhibitor, H10; a shorter distance is observed in TS-C2 (2.74 Å) than in TS1-C3 (2.87 Å). A longer O3−H10 distance in the latter can explain why intermediate I-C3 is located in the C3 attack mechanism with a remarkable negatively charged O3 atom (−0.606 au). It is also important to point out the slightly higher negative charge developed on O3 in TS-C2 (−0.546 au) by comparison with that in TS1-C3 (−0.532 au), which could help explain why the H10 atom is spontaneously transferred from TS-C2 to products in the C2 attack mechanism. The negatively charged O3 atom is stabilized, both in the TSs and in intermediate I1-C3, through hydrogen bond interactions with water molecules of the active site, as shown in Table 1. There are other interesting interactions between the inhibitor and the residues of the active site that are maintained during the full process, such as those with Asp170 and Gln171. These residues would then contribute to anchor the inhibitor to the active site. This is especially important when the covalent bond is not yet formed (reactants). The interactions between O1 and O2 of the inhibitor and His174 and Gln36 are also maintained during the reaction, becoming more intense (shorter distances in Table 1) when the group is deprotonated (products). The large deviations observed in these distances, together with the change in the interaction of O2 in TS2-C3, reveal the flexibility of the active site, thus justifying the statistical simulations performed in this study. Analysis of the time-dependent evolution of structures appearing on the QM/MM MD simulation on TS2-C3 shows that O2 of the carboxylate group can interact, alternatively, with Gln36 or His174 (see Figure S6 of the Supporting Information). Trp43 is also interacting with the inhibitor through the carbonyl O4 atom, although in some of the structures appearing in the mechanism of the attack on C3. Because of the flexibility of the active site (see the standard deviations), the interaction with Trp43 is replaced by an interaction with the polar hydrogen atom of the backbone of Ala175. Finally, as mentioned above, a new interaction is observed in products between Asn81 and the new O3-H10 hydroxyl group, as a result of the rotation of this group once the proton is completely transferred to the oxygen epoxy ring.

CONCLUSIONS

In this paper, the inhibition of FP2 by the epoxysuccinate E64 has been studied by means of MD simulations using hybrid AM1d/MM and M06-2X/MM potentials. The results have allowed us to obtain a complete picture of the possible reaction paths corresponding to the irreversible attack of Cys42 on the carbon atoms of the epoxy ring of the E64 inhibitor. According to our results, the attack of Cys42 on C2 would take place in a single step, while the attack on C3 is described as a two-step mechanism, the first step corresponding to formation of the sulfur−carbon bond, which is the rate-limiting step. In the second step of this mechanism, a hydrogen atom from the carboxylic group of the inhibitor is finally transferred to the oxygen atom of the opened epoxy ring. This step, when computed at the DFT/MM level, becomes a barrier-less process. Thus, the free energy barriers of the first mechanism and the rate-limiting step of the second are almost equivalent (12.3 and 13.6 kcal/mol for the attack on C2 and C3, respectively), which is in agreement with experimental data. Nevertheless, the inhibitor−protein complex derived from the attack on C3 appears to be much more stabilized. Analysis of averaged geometries and charges of stationary points on the QM/MM free energy surfaces has been used to rationalize the different reaction mechanisms. A thorough analysis of the inhibitor−protein interactions reveals the importance of some of the residues, such as Gln171, Asp170, Gln36, Trp43, Asn81, and His174, in anchoring the inhibitor in a proper orientation for the reaction to take place.

Any attempt to explore an alternative mechanism implying the protonation of the epoxy ring prior to the attack of cysteine on C2 or C3 of the ring, by His174, by a water molecule, or through an intramolecular transfer of a proton from the acid group at C2 as an acid, as suggested in the literature, has been unsuccessful. Finally, it is important to stress that our simulations have allowed detection of two different conformations of a productlike structure, differing in the relative orientation of E64 in the active site of the protein: a conformation similar to the initial X-ray structure (PDB entry 3BPF) with the guanidine group of E64 interacting with Tyr78 and a conformation in which the guanidine group of E64 interacts with Asp170. Analysis of our results reveals that, despite both structures being stable, the latter appears to be energeticaly favored. The flexible character of the system appears to be demonstrated, thus justifying the statistical simulations conducted in this work. Thus, these results may be useful for the rational design of new compounds with higher inhibitory activity against malaria parasites.

ASSOCIATED CONTENT

Supporting Information

Averaged AM1d/MM distances obtained from 200 ps of QM/MM MD simulation for the reactant state and product state of the reaction mechanism of inhibition of FP2 by attack of Cys42 on C2 at pH 5.5 and 7 (Table S1), averaged AM1d/MM distances obtained for key states located along the reaction mechanism of the second step of the attack of Cys42 on C3 (Table S2), time evolution of the potential energy and total energy obtained along 200 ps of the QM/MM MD simulation performed for productlike structures in two different conformations (Figure S1), AM1d/MM PMFs of the attack of sulfur on C2 (green line) or C3 (red line) obtained after 200 ps of MD starting from the X-ray conformation (Figure S2), representative snapshots of the key states of the reaction mechanism of the second step of the attack of Cys42 on C3 (protonation of O3 by intramolecular proton transfer) (Figure S3), representative snapshots of the key states of the reaction mechanism of the second step of the attack of Cys42 on C3 (protonation of O3 with participation of a water molecule) (Figure S4), PMFs of the alternative mechanisms of the inhibition of FP2 with E64, with an early transfer of a proton to O3 of the epoxide ring prior to the Cys42 attack (Figure S5), and time-dependent evolution of selected distances on the QM/MM MD simulation constrained on TS2-C3 (Figure S6). This material is available free of charge via the Internet at http://pubs.acs.org.

AUTHOR INFORMATION

Corresponding Authors

*E-mail: sferrer@uji.es.
*E-mail: moliner@uji.es.

Author Contributions

K.A. performed the bulk of computational simulations. S.M. wrote the codes and guided some of the calculations. S.M., S.F., and V.M. designed the research. K.A., S.F., and V.M. cowrote the first version of the manuscript. All the authors analyzed data, and V.M. wrote the final version of the manuscript.

Funding

This work was supported by the Spanish Ministerio de Economía y Competitividad (ref CTQ2012-36253-C03-01), Generalitat Valenciana (ref Prometeo/2009/053), Universitat Jaume I (ref P1·1B2011-23), and a predoctoral contract to K.A. from the Spanish Ministerio de Economía y Competitividad.

Notes

The authors declare no competing financial interest.

ACKNOWLEDGMENTS

We acknowledge the Servei d'Informatica, Universitat Jaume I, for the generous allotment of computer time.

REFERENCES

(1) http://www.who.int/malaria/publications/world_malaria_report_2013/report/en/index.html (2013).

(2) Jana, S., and Paliwal, J. (2007) Novel molecular targets for antimalarial chemotherapy. *Int. J. Antimicrob. Agents 30*, 4−10.

(3) Mital, A. (2007) Recent advances in antimalarial compounds and their patents. *Curr. Med. Chem. 14*, 759−773.

(4) Miller, L. H., Baruch, D. I., Marsh, K., and Doumbo, O. K. (2002) The pathogenic basis of malaria. *Nature 415*, 673−679.

(5) Singh, A., and Rosenthal, P. J. (2004) Selection of cysteine protease inhibitor-resistant malaria parasites is accompanied by amplification of falcipain genes and alteration in inhibitor transport. *J. Biol. Chem. 279*, 35236−35241.

(6) Shenai, B. R., Sijwali, P. S., Singh, A., and Rosenthal, P. J. (2000) Characterization of native and recombinant falcipain-2, a principal trophozoite cysteine protease and essential hemoglobinase of *Plasmodium falciparum*. *J. Biol. Chem. 275*, 29000−29010.

(7) Sijwali, P. S., Shenai, B. R., Gut, J., Singh, A., and Rosenthal, P. J. (2001) Expression and characterization of the *Plasmodium falciparum* haemoglobinase falcipain-3. *Biochem. J. 360*, 481−489.

(8) Marco, M., and Miguel Coteron, J. (2012) Falcipain Inhibition as a Promising Antimalarial Target. *Curr. Top. Med. Chem. 12*, 408−444.

(9) Ehmke, V., Heindl, C., Rottmann, M., Freymond, C., Schweizer, W. B., Brun, R., Stich, A., Schirmeister, T., and Diederich, F. (2011) Potent and Selective Inhibition of Cysteine Proteases from *Plasmodium falciparum* and *Trypanosoma brucei*. *ChemMedChem 6*, 273−278.

(10) Ehmke, V., Kilchmann, F., Heindl, C., Cui, K., Huang, J., Schirmeister, T., and Diederich, F. (2011) Peptidomimetic nitriles as selective inhibitors for the malarial cysteine protease falcipain-2. *MedChemComm 2*, 800−804.

(11) Ettari, R., Bova, F., Zappala, M., Grasso, S., and Micale, N. (2010) Falcipain-2 Inhibitors. *Med. Res. Rev. 30*, 136−167.

(12) Ettari, R., Micale, N., Grazioso, G., Bova, F., Schirmeister, T., Grasso, S., and Zappala, M. (2012) Synthesis and Molecular Modeling Studies of Derivatives of a Highly Potent Peptidomimetic Vinyl Ester as Falcipain-2 Inhibitors. *ChemMedChem 7*, 1594−1600.

(13) Ettari, R., Nizi, E., Di Francesco, M. E., Micale, N., Grasso, S., Zappala, M., Vicik, R., and Schirmeister, T. (2008) Nonpeptidic vinyl and allyl phosphonates as falcipain-2 inhibitors. *ChemMedChem 3*, 1030−1033.

(14) Ettari, R., Zappala, M., Micale, N., Grazioso, G., Giofre, S., Schirmeister, T., and Grasso, S. (2011) Peptidomimetics containing a vinyl ketone warhead as falcipain-2 inhibitors. *Eur. J. Med. Chem. 46*, 2058−2065.

(15) Gonzalez, F. V., Izquierdo, J., Rodriguez, S., McKerrow, J. H., and Hansell, E. (2007) Dipeptidyl-α,β-epoxyesters as potent irreversible inhibitors of the cysteine proteases cruzain and rhodesain. *Bioorg. Med. Chem. Lett. 17*, 6697−6700.

(16) Hansen, G., Heitmann, A., Witt, T., Li, H., Jiang, H., Shen, X., Heussler, V. T., Rennenberg, A., and Hilgenfeld, R. (2011) Structural Basis for the Regulation of Cysteine-Protease Activity by a New Class of Protease Inhibitors in *Plasmodium*. *Structure 19*, 919−929.

(17) Kerr, I. D., Lee, J. H., Pandey, K. C., Harrison, A., Sajid, M., Rosenthal, P. J., and Brinen, L. S. (2009) Structures of falcipain-2 and falcipain-3 bound to small molecule inhibitors: Implications for substrate specificity. *J. Med. Chem. 52*, 852−857.

(18) Wang, S. X., Pandey, K. C., Somoza, J. R., Sijwali, P. S., Kortemme, T., Brinen, L. S., Fletterick, R. J., Rosenthal, P. J., and McKerrow, J. H. (2006) Structural basis for unique mechanisms of folding and hemoglobin binding by a malarial protease. *Proc. Natl. Acad. Sci. U.S.A. 103*, 11503−11508.

(19) Suzuki, K., Tsuji, S., and Ishiura, S. (1981) Effec of Ca^{2+} on the inhibition of calcium-activated neutral protease by leupeptin, anti-pain and epoxysuccinate derivates. *FEBS Lett. 136*, 119−122.

(20) Hanada, K., Tamai, M., Yamagishi, M., Ohmura, S., Sawada, J., and Tanaka, I. (1978) Isolation and characterization of E-64, a new thiol protease inhibitor. *Agric. Biol. Chem. 42*, 523−528.

(21) Hanada, K., Tamai, M., Ohmura, S., Sawada, J., Seki, T., and Tanaka, I. (1978) Structure and synthesis of E-64, a new thiol protease inhibitor. *Agric. Biol. Chem. 42*, 529−536.

(22) James, K. E., Asgian, J. L., Li, Z. Z., Ekici, O. D., Rubin, J. R., Mikolajczyk, J., Salvesen, G. S., and Powers, J. C. (2004) Design, synthesis, and evaluation of aza-peptide epoxides as selective and potent inhibitors of caspases-1, -3, -6, and-8. *J. Med. Chem. 47*, 1553−1574.

(23) Roush, W. R., Gonzalez, F. V., McKerrow, J. H., and Hansell, E. (1998) Design and synthesis of dipeptidyl α',β'-epoxy ketones, potent irreversible inhibitors of the cysteine protease cruzain. *Bioorg. Med. Chem. Lett. 8*, 2809−2812.

(24) Matsumoto, K., Yamamoto, D., Ohishi, H., Tomoo, K., Ishida, T., Inoue, M., Sadatome, T., Kitamura, K., and Mizuno, H. (1989) Mode of bindinf of E64-C, a potent thiol protease inhibitor, to papain as determined by X-ray crystals analysis of the complex. *FEBS Lett. 245*, 177−180.

(25) Yabe, Y., Guillaume, D., and Rich, D. H. (1988) Irreversible inhibition of papain by epoxysuccinyl peptides. Carbon-13 NMR characterization of the site of alkylation. *J. Am. Chem. Soc. 110*, 4043−4044.

(26) Powers, J. C., Asgian, J. L., Ekici, O. D., and James, K. E. (2002) Irreversible inhibitors of serine, cysteine, and threonine proteases. *Chem. Rev. 102*, 4639−4750.

(27) Ghosh, R., Chakraborty, S., Chakrabarti, C., Dattagupta, J. K., and Biswas, S. (2008) Structural insights into the substrate specificity and activity of ervatamins, the papain-like cysteine proteases from a tropical plant, *Ervatamia coronaria*. *FEBS J. 275*, 421−434.

(28) Kim, M. J., Yamamoto, D., Matsumoto, K., Inoue, M., Ishida, T., Mizuno, H., Sumiya, S., and Kitamura, K. (1992) Crystal-structure of papain-E64-C complex-binding diversity of E64-C to papain S(2) and S(3) subsites. *Biochem. J. 287*, 797−803.

(29) Yamamoto, A., Tomoo, K., Matsugi, K., Hara, T., In, Y., Murata, M., Kitamura, K., and Ishida, T. (2002) Structural basis for development of cathepsin B-specific noncovalent-type inhibitor: Crystal structure of cathepsin B-E64c complex. *Biochim. Biophys. Acta 1597*, 244−251.

(30) Yamamoto, D., Matsumoto, K., Ohishi, H., Ishida, T., Inoue, M., Kitamura, K., and Mizuno, H. (1991) Refined X-ray structure of papain·E-64-C complex at 2.1-Å resolution. *J. Biol. Chem. 266*, 14771−14777.

(31) Zhao, B. G., Janson, C. A., Amegadzie, B. Y., Dalessio, K., Griffin, C., Hanning, C. R., Jones, C., Kurdyla, J., McQueney, M., Qiu, X. Y., Smith, W. W., and AbdelMeguid, S. S. (1997) Crystal structure of human osteoclast cathepsin K complex with E-64. *Nat. Struct. Biol. 4*, 109−111.
(32) Mladenovic, M., Junold, K., Fink, R. F., Thiel, W., Schirmeister, T., and Engels, B. (2008) Atomistic insights into the inhibition of cysteine proteases: First QM/MM calculations clarifying the regiospecificity and the inhibition potency of epoxide- and aziridine-based inhibitors. *J. Phys. Chem. B 112*, 5458−5469.
(33) Bihovsky, R. (1992) Reactions of α,β-epoxy carbonyl-compounds with methanethiolate-regioselectivity and rate. *J. Org. Chem. 57*, 1029−1031.
(34) Rich, D. H. (1986) *Proteinase Inhibitors*, Elsevier, Amsterdam.
(35) Varughese, K. I., Ahmed, F. R., Carey, P. R., Hasnain, S., Huber, C. P., and Storer, A. C. (1989) Crystal-structure of a papain-structure of a papain-E64 complex. *Biochemistry 28*, 1330−1332.
(36) Meara, J. P., and Rich, D. H. (1996) Mechanistic studies on the inactivation of papain by epoxysuccinyl inhibitors. *J. Med. Chem. 39*, 3357−3366.
(37) Warshel, A., and Levitt, M. (1976) Theoretical studies of enzymic reactions: Dielectric, electrostatic and steric stabilization of carbonium-ion reaction lysozyme. *J. Mol. Biol. 103*, 227−249.
(38) Martí, S., Roca, M., Andres, J., Moliner, V., Silla, E., Tuñón, I., and Bertran, J. (2004) Theoretical insights in enzyme catalysis. *Chem. Soc. Rev. 33*, 98−107.
(39) Senn, H. M., and Thiel, W. (2009) QM/MM Methods for Biomolecular Systems. *Angew. Chem., Int. Ed. 48*, 1198−1229.
(40) van der Kamp, M. W., and Mulholland, A. J. (2013) Combined Quantum Mechanics/Molecular Mechanics (QM/MM) Methods in Computational Enzymology. *Biochemistry 52*, 2708−2728.
(41) Hogg, T., Nagarajan, K., Herzberg, S., Chen, L., Shen, X., Jiang, H., Wecke, M., Blohmke, C., Hilgenfeld, R., and Schmidt, C. L. (2006) Structural and functional characterization of falcipain-2, a hemoglobinase from the malarial parasite *Plasmodium falciparum*. *J. Biol. Chem. 281*, 25425−25437.
(42) Field, M. J., Albe, M., Bret, C., Proust-De Martin, F., and Thomas, A. (2000) The Dynamo library for molecular simulations using hybrid quantum mechanical and molecular mechanical potentials. *J. Comput. Chem. 21*, 1088−1100.
(43) Bas, D. C., Rogers, D. M., and Jensen, J. H. (2008) Very fast prediction and rationalization of pK_a values for protein-ligand complexes. *Proteins: Struct., Funct., Bioinf. 73*, 765−783.
(44) Li, H., Robertson, A. D., and Jensen, J. H. (2005) Very fast empirical prediction and rationalization of protein pK_a values. *Proteins: Struct., Funct., Bioinf. 61*, 704−721.
(45) Olsson, M. H. M., Sondergaard, C. R., Rostkowski, M., and Jensen, J. H. (2011) PROPKA3: Consistent Treatment of Internal and Surface Residues in Empirical pK_a Predictions. *J. Chem. Theory Comput. 7*, 525−537.
(46) Nam, K., Cui, Q., Gao, J., and York, D. M. (2007) Specific reaction parametrization of the AM1/d Hamiltonian for phosphoryl transfer reactions: H, O, and P atoms. *J. Chem. Theory Comput. 3*, 486−504.
(47) Jorgensen, W. L., Maxwell, D. S., and TiradoRives, J. (1996) Development and testing of the OPLS all-atom force field on conformational energetics and properties of organic liquids. *J. Am. Chem. Soc. 118*, 11225−11236.
(48) Jorgensen, W. L., Chandrasekhar, J., Madura, J. D., Impey, R. W., and Klein, M. L. (1983) Comparison of simple potential functions for simulating liquid water. *J. Chem. Phys. 79*, 926−935.
(49) Field, M. J., Bash, P. A., and Karplus, M. (1990) A combined quantum-mechanical and molecular mechanical potential for molecular-dynamics simulations. *J. Comput. Chem. 11*, 700−733.
(50) Singh, U. C., and Kollman, P. A. (1986) A combined abinitio quantum-mechanical and molecular mechanical method for carryng out simulations on complex molecular-systems: Applications to the CH3CL + CL- Exchange-reaction and gas-phase protonation of polyethers. *J. Comput. Chem. 7*, 718−730.
(51) Martí, S., Moliner, V., and Tuñón, I. (2005) Improving the QM/MM description of chemical processes: A dual level strategy to explore the potential energy surface in very large systems. *J. Chem. Theory Comput. 1*, 1008−1016.
(52) Grazioso, G., Legnani, L., Toma, L., Ettari, R., Micale, N., and De Micheli, C. (2012) Mechanism of falcipain-2 inhibition by α,β-unsaturated benzo 1,4-diazepin-2-one methyl ester. *J. Comput.-Aided Mol. Des. 26*, 1035−1043.
(53) Kumar, S., Bouzida, D., Swendsen, R. H., Kollman, P. A., and Rosenberg, J. M. (1992) The weighted histogram analysis method for free-energy calculations on biomolecules. 1. The method. *J. Comput. Chem. 13*, 1011−1021.
(54) Torrie, G. M., and Valleau, J. P. (1977) Non-physical sampling distributions in monte-carlo free-energy estimation: Umbrella sampling. *J. Comput. Phys. 23*, 187−199.
(55) Ruiz-Pernia, J. J., Silla, E., Tuñón, I., Martí, S., and Moliner, V. (2004) Hybrid QM/MM potentials of mean force with interpolated corrections. *J. Phys. Chem. B 108*, 8427−8433.
(56) Chuang, Y. Y., Corchado, J. C., and Truhlar, D. G. (1999) Mapped interpolation scheme for single-point energy corrections in reaction rate calculations and a critical evaluation of dual-level reaction path dynamics methods. *J. Phys. Chem. A 103*, 1140−1149.
(57) Zhao, Y., and Truhlar, D. G. (2008) The M06 suite of density functionals for main group thermochemistry, thermochemical kinetics, noncovalent interactions, excited states, and transition elements: Two new functionals and systematic testing of four M06-class functionals and 12 other functionals. *Theor. Chem. Acc. 120*, 215−241.
(58) Hehre, W. J., Radom, L., von R. Schleyer, P., and Pople, J. A. (1986) *Ab Initio Molecular Orbital Theory*, John Wiley & Sons, New York.
(59) Lynch, B. J., Zhao, Y., and Truhlar, D. G. (2003) Effectiveness of Diffuse Basis Functions for Calculating Relative Energies by Density Functional Theory. *J. Phys. Chem. A 107*, 1384−1388.
(60) Frisch, M. J., Trucks, G. W., Schlegel, H. B., Scuseria, G. E., Robb, M. A., Cheeseman, J. R., Scalmani, G., Barone, V., Mennucci, B., Petersson, G. A., Nakatsuji, H. C., Li, X., Hratchian, H. P., Izmaylov, A. F., Bloino, J., Zheng, G., Sonnenberg, J. L., Hada, M., Ehara, M., Toyota, K., Fukuda, R., Hasegawa, J., Ishida, M., Nakajima, T., Honda, Y., Kitao, O., Nakai, H., Vreven, T., Montgomery, J. A., Jr., Peralta, J. E., Ogliaro, F., Bearpark, M., Heyd, J. J., Brothers, E., Kudin, K. N., Staroverov, V. N., Kobayashi, R., Normand, J., Raghavachari, K., Rendell, A., Burant, J. C., Iyengar, S. S., Tomasi, J., Cossi, M., Rega, N., Millam, N. J., Klene, M., Knox, J. E., Cross, J. B., Bakken, V., Adamo, C., Jaramillo, J., Gomperts, R., Stratmann, R. E., Yazyev, O., Austin, A. J., Cammi, R., Pomelli, C., Ochterski, J. W., Martin, R. L., Morokuma, K., Zakrzewski, V. G., Voth, G. A., Salvador, P., Dannenberg, J. J., Dapprich, S., Daniels, A. D., Farkas, Ö., Foresman, J. B., Ortiz, J. V., Cioslowski, J., and Fox, D. J. (2009) *Gaussian 09*, revision A.1, Gaussian Inc., Wallingford, CT.